Hindawi

Research Article

Evaluation of Silver Nanoparticles Based on Fresh Cocoa Pods (*Theobroma Cacao*) Extracts as New Potential Electrode Material

Alex Vincent Somba,[1,2] Evangéline Njanja,[1] Gullit Deffo,[1] Cyrille Ghislain Fotsop,[1,3] Kevin Yemele Tajeu,[1] Armel Florian Tchangou Njiemou [ID],[2] François Eya'ane Meva [ID],[2] and Theophile Kamgaing [ID][1]

[1]*Electrochemistry and Chemistry of Materials, Department of Chemistry, Faculty of Sciences, University of Dschang, P.O. Box 67, Dschang, Cameroon*
[2]*Department of Pharmaceutical Sciences, Faculty of Medicine and Pharmaceutical Sciences, University of Douala, P.O. Box 2701, Douala, Cameroon*
[3]*Institute of Chemistry, Faculty of Process and Systems Engineering, Universitätsplatz 2, Magdeburg 39106, Germany*

Correspondence should be addressed to François Eya'ane Meva; mevae@daad-alumni.de and Theophile Kamgaing; theokamgaing@yahoo.fr

This work focuses on the synthesis of silver nanoparticles using fresh cocoa pods from the "*Theobroma cacao*" extract plant through the reduction of silver ions (Ag^+) into Ag (0) by a green chemistry process, subsequently used as an electrode material. Reaction factors such as pH, incubation time, and silver ion concentration were optimized during the formation of nanoparticles. The synthesized nanoparticles were characterized by ultraviolet spectrophotometry (UV-Vis), Fourier transform infrared spectroscopy (FT-IR), powder X-ray diffraction (PXRD), scanning electron microscopy (SEM), and energy dispersive X-ray spectrometry (EDX) analysis. Once drop coating was applied on the glassy carbon electrode (GCE), the resulting film was characterized using cyclic voltammetry (CV) and electrochemical impedance spectroscopy (EIS). The results show that silver nanoparticles have been well synthesized and can find applications as electrode materials for simultaneous determination of ascorbic acid and uric acid in aqueous solution.

1. Introduction

Nanotechnology is an area of extensive research which plays an important role in the manufacturing of new materials for application in nano-health delivery systems [1]. Nanomaterials, specifically metallic nanoparticles made of single or multiple metals (alloy nanoparticles), have significant interest in various fields ranging from materials science to biotechnology [2–4]. They are widely used in medicine for antimicrobial medical products and personal care, in industry for the manufacture of building materials and wastewater filtration, in food processing, cosmetics, and in clothing manufacturing [5, 6]. Among those metallic nanoparticles, silver nanoparticles (AgNPs) are mostly used

because nanometric silver is produced in good quantities. Silver nanoparticles are synthesized under various approaches, including chemical and biological methods [7]. The chemical approach requires styling agents (chemicals) for the stabilization of the nanoparticles which are toxic to organisms and the environment. Thus, the biocompatibility of the resulting AgNPs is too low for application in biological systems [8]. The biological method uses biological agents such as actinomycetes, bacteria, algae, fungi, plants, viruses, and yeasts [9]. Moreover, not all biological entities can be used for the synthesis of nanoparticles because of their enzymatic activities and intrinsic metabolic processes. Therefore, an appropriate selection of the biological entity is needed to produce nanoparticles with interesting properties

such as specific size and morphology. For both chemical and biological methods, the use of costly chemicals or reagents is required, and the lifetime of some resulting nanoparticles is low [10]. Therefore, the green chemistry process is proposed today by researchers as an alternative for the synthesis of silver nanoparticles, which is eco-friendly and sustainable [8]. The literature survey shows some work published recently for the synthesis of AgNPs by a green chemistry process through the use of plant extracts of *Megaphrynium macrostachyum* [11], *Eucalyptus hybrid* Myrtaceae [12], *Helianthus annuus*, Asteraceae [13], *Oryza sativa*, Poaceae [14], *Mentha piperita*, and Lamiaceae [15]. However, the above AgNPs synthesized have never been used in the electroanalysis domain. Therefore, in the present work, apart from having as novelty the synthesis of silver nanoparticles from fresh cocoa pods (*Theobroma Cacao*), this work would show for the first time that it is possible to use the resulting AgNPs as electrode material for the analysis of pathological compounds such as ascorbic acid (AA) and uric acid (UA), which are important and urgent analytes to be daily tested clinically.

Ascorbic acid and uric acid are coexisting constituents of pathological samples, which always appear at the same potential, making it difficult to separate them for their identification. In physiological samples, the normal range of ascorbic acid is 11.5–115 μmol/L and that of uric acid is 160–500 μmol/L [16, 17]. The amount of these species is a marker of the health condition of human beings, as both the low level as well as the high level can cause different adverse health effects. Even if ascorbic acid is generally well tolerated by the humans in the normal range of 0.6–2 mg/dL, large doses may cause gastrointestinal discomfort, headache, trouble in sleeping, and flushing of the skin [16]. Unusual concentrations of uric acid (high-level-induced hyperuricemia) result in diseases such as arthritis, diabetes, gout, high blood pressure, hypertension, Lesch–Nyhan syndrome, neurological diseases, and obesity. Low levels of uric acid (low-level induced hypouricemia) in serum can result in cardiovascular disease, multiple sclerosis, Parkinson's, schizophrenia, and scurvy [18, 19].

Given the above healthy effects and the industrial and biomedical importance of ascorbic acid and uric acid, it is important to develop a method for the daily monitoring of products consumed by humans. This passes through the elaboration of point-of-care testing (POCT) device for clinical applications. Several works have been published on this aim [16–20], but due to the lack of good stability, sensitivity, and electrocatalytic ability for the separation of pathological compounds, the research in this aspect is still ongoing. The present work has following objectives: 1. To develop a green method for the synthesis of silver nanoparticles from *Theobroma cacao* extracts. 2. To use the resulting AgNPs as electrode material to test their electrocatalytic ability for the separation of ascorbic acid and uric acid. The societal implication of this work would then be the valorization of the plant, since, due to their large availability, they are usually considered waste for farms or as firewood.

2. Reagents, Materials, and Methods

2.1. Reagents and Materials.
Commercially obtained chemicals were used without further purification. Silver nitrate (AgNO$_3$, 98%), sodium hydroxide (NaOH, 99%), sulfuric acid (H$_2$SO$_4$, 98%), ethanol (C$_2$H$_5$OH, 99.99%), alumina (Al$_2$O$_3$, 98%), ascorbic acid (C$_6$H$_8$O$_6$, 99%), and uric acid (C$_5$H$_4$O$_3$N$_4$, 99%) were purchased from Sigma Aldrich Germany and K$_3$Fe(CN)$_6$ (98%), K$_4$Fe(CN)$_6$ (98%), [Ru(NH$_3$)$_6$] Cl$_3$ (98%), Fe (MeOH)$_2$ (98%), hydrochloric acid (HCl, 36%), and boric acid (H$_3$BO$_3$, 99%) were obtained from Prolabo and Acros Organics, respectively.

2.2. Collection of Material and Preparation of Extracts.
Theobroma cocoa (Figure 1) was collected in the Santchou district (West region, Cameroon) and authenticated at the National Herbarium of Cameroon, compared to the reference sample of the herbarium according to the reference *Theobroma cocoa* Linn No. 60111/HNC. Fresh cocoa pods (*Theobroma cacao*) were first washed with water, then cut into very small sizes, cleaned, and dried at room temperature. 15 g of dried cocoa pods (CP) were introduced into a flask of water (W) (ratio 10 : 1 W/CP) previously heated to 80°C for 10 min. The mixture was stirred for 5 min. After being cooled to room temperature, the mixture was sieved under cotton, and the resulting extract was filtered using Whatman filter paper Nr1 and stored in the refrigerator at 4°C.

2.3. Synthesis of Silver Nanoparticles.
The procedure used is adapted to that proposed by Eya'ane et al. [21] with slight modifications [21]. In practice, different solutions of silver nitrate (1 mM, 2 mM, and 3 mM in 100 mL) were prepared and stored in tightly closed bottles to prevent the oxidation of silver. Subsequently, the aqueous extracts of *Theobroma cocoa* (TCC) were introduced into several vials numbered A to C, followed by the addition of silver nitrate solution in the volume ratio 5 : 1 (AgNO$_3$/TCC); the mixture was left at room temperature for the bioreduction of silver ion. The dark incubation time was set for 30 min, 1 h, 24 h, and 48 h to minimize the photoactivation of silver nitrate; the pH of the solution was adjusted to 6, 8, and 10 using 0.1 M NaOH or H$_2$SO$_4$. After each incubation time, the nanoparticle solutions were centrifuged at 6000 rpm for 1 h and washed twice with distilled water and once with ethanol (99.99%). The final product obtained was dried in an oven at 60°C for 24 h and stored in an eppendorf for future uses.

2.4. Physicochemical Characterization Techniques and Apparatus.
The formation of silver nanoparticles was monitored after each incubation time, recording the UV-visible spectrum of the reaction mixture using a UV line 9100 UV-vis spectrophotometer. The presence of various functional groups was identified using FT-IR spectroscopy at ambient temperatures in the range of 4000 to 600 cm^{-1} with a Bruker Vertex 70. Scanning electron microscope (SEM) images were taken using the Zeiss SIGMA FE-SEM device to study the texture of the formed nanoparticles, and EDX

FIGURE 1: Fresh cocoa pods harvested in a field located in the district of Santchou (West region Cameroon).

spectra were carried out using a Zeiss SIGMA FE-SEM device to find the chemical elements and morphology of the nanoparticles based on extracts of fresh cocoa pods. The elemental analysis was carried out using a thermo Scientific-flash 2000; the analysis by XRD was carried out at room temperature using a Bruker-AXS D8 X-ray diffractometer.

2.5. Electrochemical Procedure and Equipment. Prior to its modification, the glassy carbon electrode (GCE) was polished with different sizes of alumina powder (1; 0.3, and $0.05 \mu m$ sizes) and then sonicated in a 1 : 1 ethanol-water solution for 5 min. 5 mg of the synthesized nanoparticles were dispersed with ultrasound for 10 min in 1 mL of distilled water. Then $5 \mu L$ of AgNP suspension were then drop-coated on the surface of the clean GCE and dried at 50°C. The obtained electrode, namely, GCE/AgNPs, was used as a working electrode for the simultaneous determination of ascorbic acid and uric acid. For comparison, the bare GCE was also used for that purpose. Platinum wire and Ag/Ag^+ were used as counter and pseudo-reference electrodes, respectively. Cyclic voltammetry (CV) and electrochemical impedance spectroscopy (EIS) measurements were performed using a PalmSens potentiostat equipped with the PS Trace software. Voltammograms were recorded with potential ranges of −0.4 V to 0.6 V, −0.5 V to 0.2 V, and 0.4 V to 0.7 V for $[Fe (CN)_6]^{3-}$, $[Ru (NH_3)_6]^{3+}$ and $[Fe (MeOH)_2]$, respectively, at a concentration of 5×10^{-3} M, with a scan rate of 20 mV/s. EIS was performed in a solution of 0.1 M KCl, 10^{-3} M ions $[Fe (CN)6]^{3/4-}$ with a frequency range of 0.1 Hz to 1000 Hz at a potential of 0.2 V. For the simultaneous determination of ascorbic acid and uric acid, 10^{-4} M of their mixture was prepared in Briton Robinson buffer at pH 7, and the voltammograms were recorded in the potential range from 0.0 V to 1.80 V.

3. Results and Discussion

3.1. Determination of the Concentration of Nanoparticles in Solution. The nanoparticles concentration was determined by centrifugation, according to Eya'ane et al. [21]; inside three tubes, 30 mL solutions of the nanoparticles obtained at pHs 6, 8, and 10 were centrifuged for 30 min. A large amount of nanoparticles was produced at pH 10 compared to the

quantities obtained at pH 6 and 8. Table 1 summarizes the concentrations of nanoparticles in each solution. The study confirmed that basic pH is favorable for the synthesis of nanoparticle-mediated plant extracts. This can be explained by the fact that several metabolites of the extract reacted at this pH 10 for the reduction of silver ions.

3.2. Physico-Chemical Characterization of Silver Nanoparticles Based on Theobroma cocoa

3.2.1. Visual Observation of Synthesized Silver Nanoparticles. The extract of fresh cocoa pods was subjected to incubation in contact with silver ions of concentration 1 mM in proportions 5 : 1. A visual observation followed by the UV-Vis measurement was made. Initially, the extract was colorless, but after 30 min of stirring the silver solution with *Theobroma cocoa* extract, the solution changed from colorless to pale yellow (Figure 2(b)), then to brown yellow (Figure 2(c) and (d)), which suggests the formation of nanoparticles [21]. Cocoa pods are made up of several secondary metabolites such as saponins, cellulose, flavonoids, tannins, triterpenes, and steroids [22]. These secondary metabolites are the origin of the bioreduction of the Ag^+ ion into Ag^0 to form intermediate quinones.

3.2.2. UV-Visible Spectral Analysis. To optimize the synthesis of nanoparticles, the UV-Vis spectra of fresh cocoa pod extracts, silver nitrate solution, and its mixture were recorded (Figure 3). Different incubation times (30 min, 1 h, 24 h, and 48 h), pH 6, 8, and 10, and silver nitrate concentrations of 1 mM, 2 mM, and 3 mM were used. The solutions exhibit a 400 nm plasmon resonance signal that indicates the presence of nanoparticles. This value is consistent with the plasmon resonance obtained using plants and silver ion [21].

At pH 6 (Figure 4(a)), the plasmonic resonance absorbance increases with the incubation time, which is due to the increase of nanoparticle density in the solution [21]. They are located between 423 and 436 nm, which is consistent with the formation of silver nanoparticles. At 48 h of incubation time, the curve shows signs of agglomeration with the presence of peaks (Figures 4(a)–4(c)). This suggests that the secondary metabolites have reacted totally and the nanoparticles started to grow with different kinetics due to the

TABLE 1: Determination of the nanoparticle concentration of solutions.

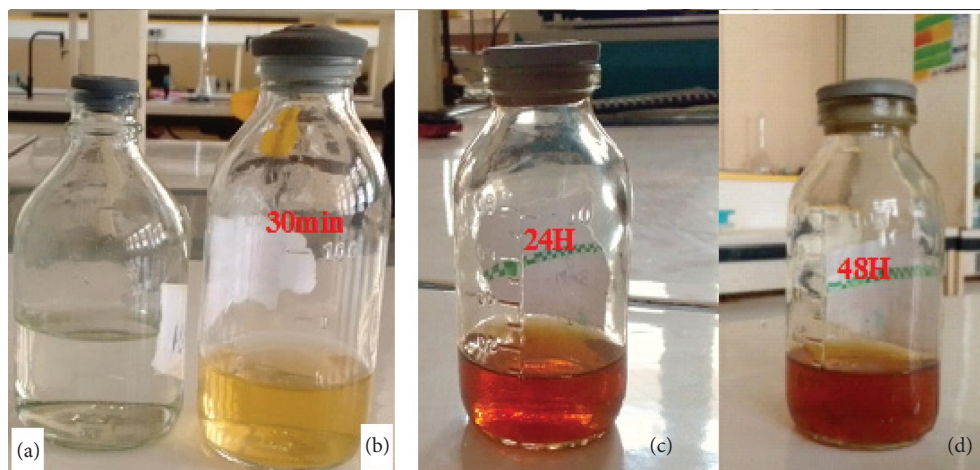| pH of solutions	Mass of particles (g)	Conc. of nanoparticles (μg/ml)
pH 6	0.0035	111.67
pH 8	0.0045	150.0
pH 10	0.0055	183.33

FIGURE 2: Aqueous extract of fresh cocoa pod (a) and of silver nanoparticles after 30 min incubation time (b); after 24 h (c); and after 48 h (d).

Silver nitrate
Silver nitrate +Theobroma cacao extract
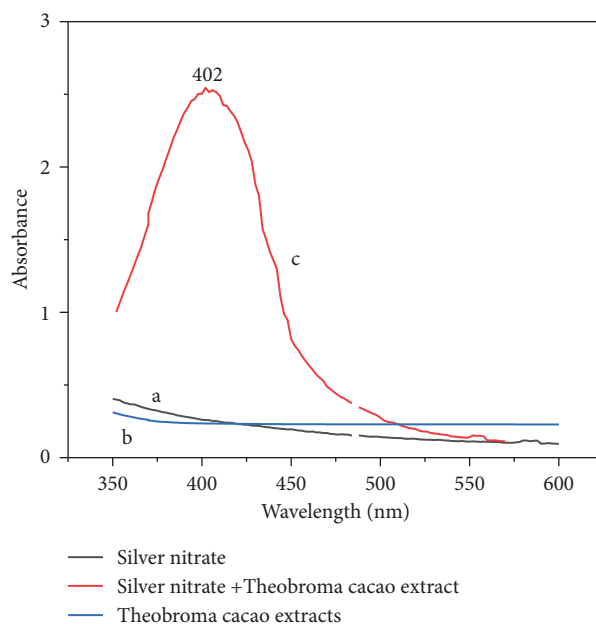Theobroma cacao extracts

FIGURE 3: UV-Vis spectra of (a) silver nitrate solution, (b) fresh cocoa pod extract solutions, and (c) the mixture of silver nitrate solution and fresh cocoa pod aqueous extract.

Brownian movement. At higher silver nitrate concentrations of 3 mM (pH 6), all curves show signs of agglomeration.

At 2 mM (Figure 4(b)), the formation of silver nanoparticles is slow compared to 1 mM and 3 mM. In general, it was observed that surface plasmon resonance bands increase with Ag^+ ion concentration [23, 24]. This could be explained by the fact that there is strong competition between the reducing molecules, which play an additional role as

nanoparticle stabilizers. Chandran and collaborators using aloevera leaves in [25] pointed out that the concentration of the reaction medium could considerably influence the shape of the nanoparticles [19]. As postulated by Mie's theory, spherical nanoparticles appear as a single plasmon resonance surface band in the absorption spectra. Furthermore, anisotropic particles exhibit two or more bands, depending on the shape of the particles [26]. These bands correspond to the
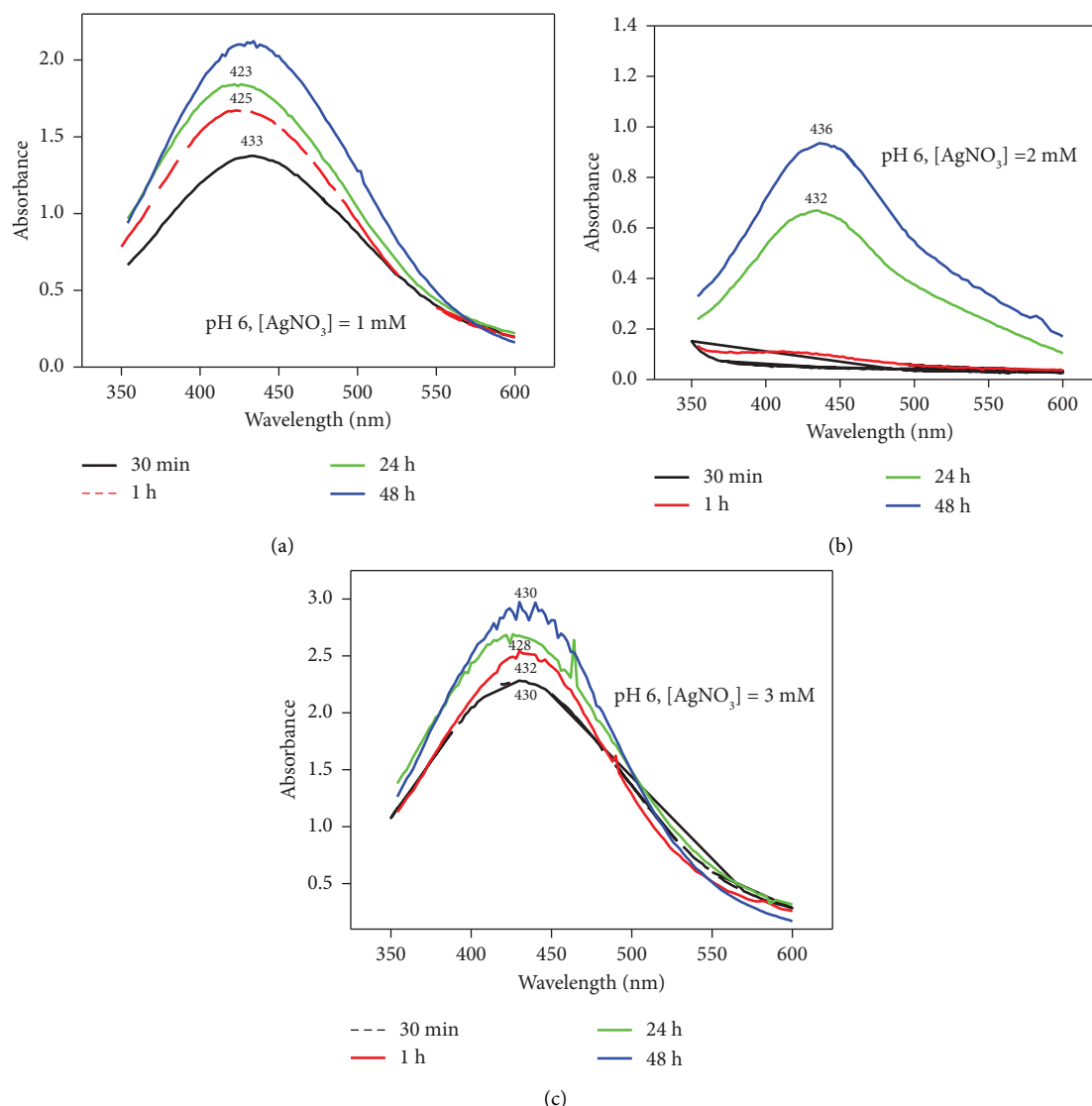
Figure 4: Plasmon resonance obtained at pH 6, incubation times of 30 min, 1 h, 24 h, and 48 h, and Ag^+ concentrations of 1 mM (a), 2 mM (b), and 3 mM (c).

appearance of a polydispersion due to the fact that the particles react with each other, but also to the simultaneous formation of particles of different nature such as Ag and AgCl [21]. A similar observation was made with the pH adjusted to 8 and 10 (Figure 5). The results obtained confirm that more nanoparticles are formed when the pH, the concentration of silver nitrate, and the incubation time increase.

3.2.3. Characterization by the FT-IR Spectroscopy.

To study the different functional groups of metabolites at the surface of nanosilver, we characterized the nanoparticles by the FT-IR spectroscopy, and the results are shown in Figure 6. The FT-IR spectrum of raw cocoa pod powder (Figure 6(a)) shows a broad band that appears in the region of $3600\,cm^{-1}$ to $3000\,cm^{-1}$ with a maximum of around $3398\,cm^{-1}$. This maximum is attributable to the stretching of hydroxyl group (−OH) of carboxyl and phenol in lignin or cellulose. The two bands observed at $1765\,cm^{-1}$ and $1612\,cm^{-1}$ were attributed, respectively, to the elongation vibrations of C=O and C=C, characteristic of the carboxylic acid metabolites. A wide band also appears between $1750\,cm^{-1}$ and $1000\,cm^{-1}$ with a maximum of $1031\,cm^{-1}$ attributed to the C-O stretching vibration in the phenol, acid, and lactone groups [27]. In the spectra of the nanoparticles (Figure 6(b)), the peaks situated at $1612\,cm^{-1}$ and $1031\,cm^{-1}$ of fresh *Theobroma cocoa* pods are displaced to lower frequencies $1525\,cm^{-1}$ and $1010\,cm^{-1}$, respectively. Furthermore, the –OH peak observed at $3398\,cm^{-1}$ in the raw pods is absent in the spectra of the nanomaterial, indicating that Ag^+ ions have been reduced by the hydroxyl group of the molecule in the extract. This shifting to lower frequencies indicates the adsorption of C-O, C=O, and C=C groups of alcohol and carboxylic acid metabolites of *Theobroma cocoa* extract to the surface of the silver nanoparticles [27].

3.2.4. Characterization by SEM.

Scanning electron microscopy was performed to determine the morphology of both raw cocoa pods (A) and AgNPs (B) and the size
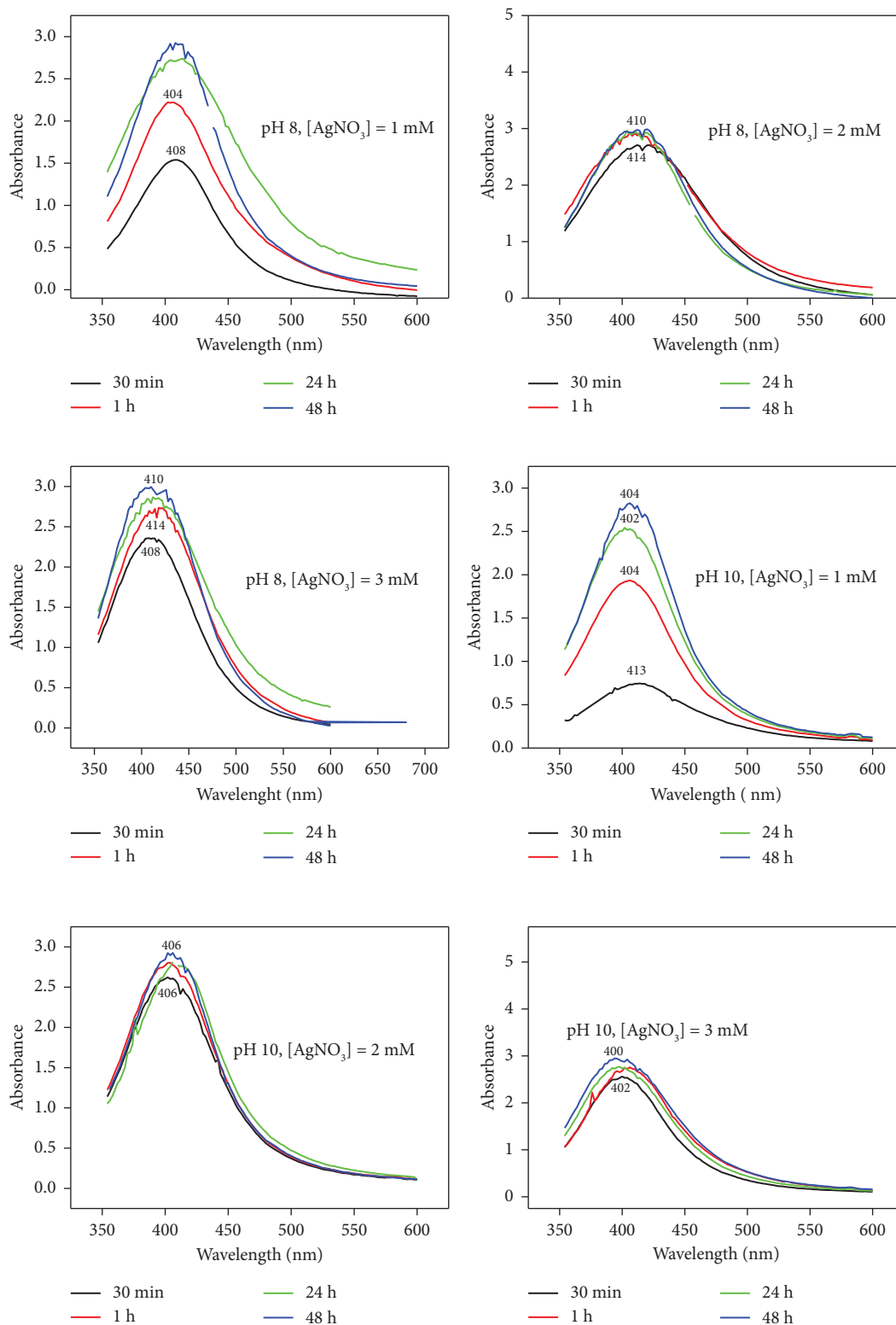
FIGURE 5: UV-Vis spectra monitoring the formation of nanoparticles at pH 8 and 10, 1 mM, 2 mM, and 3 mM Ag$^+$; during 30 min, 1 h, 24 h, and 48 h of incubation.

distribution (nm) of AgNPs. The results of these analyzes are shown in Figure 7. The image of the *Theobroma cacao* pod (Figure 7(a)) shows that there are no holes or cavities on the surface of the biomass. This result can be explained by the

high content of cellulose and the low content of lignin in the cocoa pods [28]. From Figure 7(b), spherical aggregates of silver nanoparticles are observed. SEM also shows the presence of microporosity in the nanomaterial. The
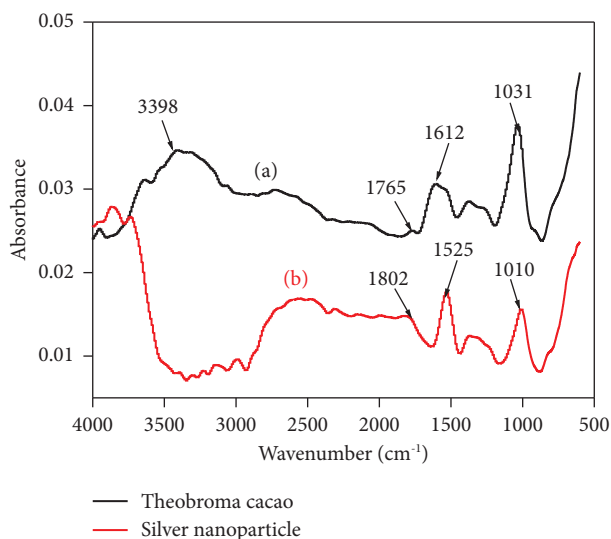
FIGURE 6: FT-IR spectra of (a) fresh *Theobroma cocoa* pods and (b) Ag-NPs.
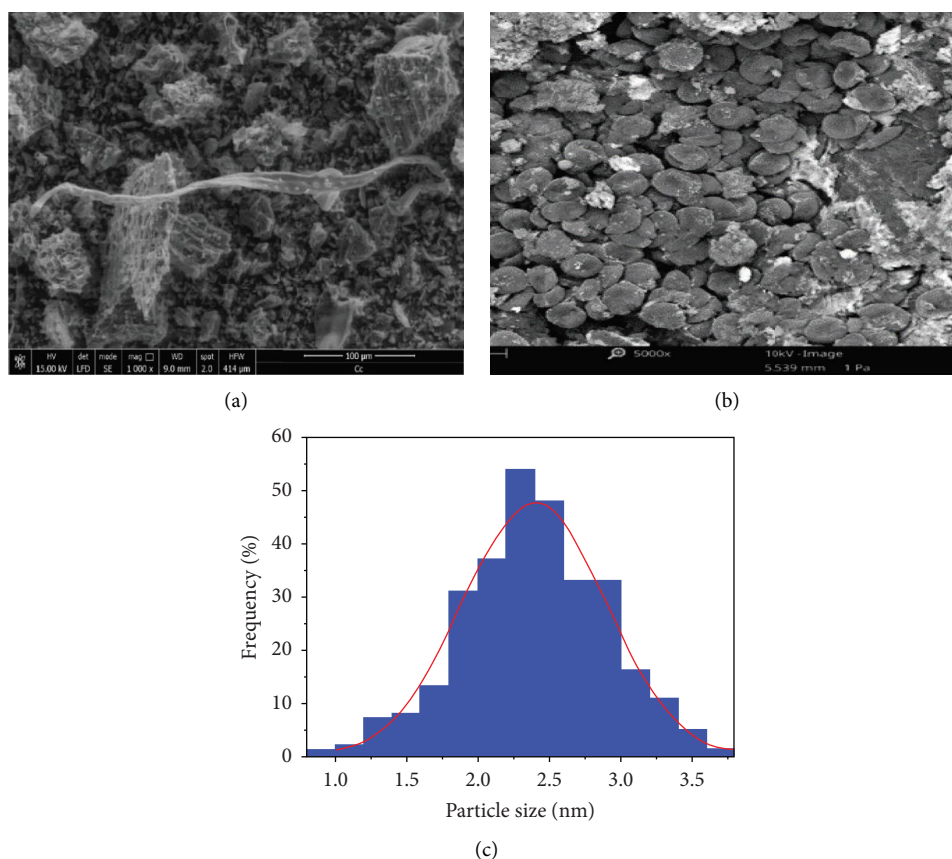

(a)

(b)

(c)

FIGURE 7: Scanning electron microscopy of fresh cocoa pods (a) and silver nanoparticles synthesized from fresh cocoa pod extract (b) and size distribution (nm) of AgNPs (c).

agglomerations of nanoparticles observed form voids (interstices). Thus, the bioreduction of silver ions by reducing agents present in fresh cocoa pod extract is effective in creating voids or pores, leading to a porous structure. The resulting histogram representing the size distribution of the particles was obtained by digital analysis of an image containing at least 80 particles (Figure 7(c)). There is a variation in particle size with nearly 5% of particles in the 1 nm range, 10% of particles in the 1.5 nm range, 25% of particles in the 2 nm range, 45% in the 2.3 nm range, and 12% in the 3 nm range. A very small percentage of nanoparticles exist in the long 3.5 nm range.
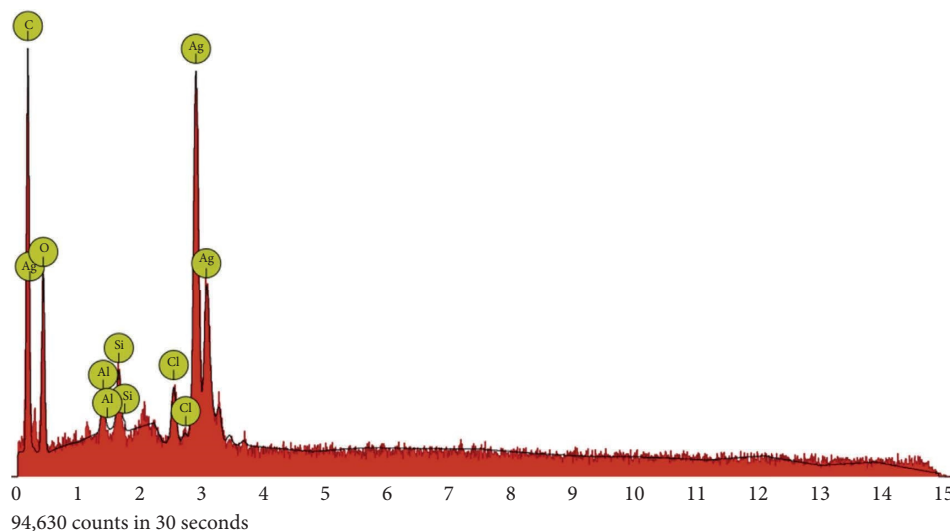
FIGURE 8: EDX spectrum of silver nanoparticles based on extracts of fresh cocoa pods.

3.2.5. EDX Analysis of Silver Nanoparticles. Figure 8 shows the EDX spectrum of silver nanoparticles based on the extracts of fresh cocoa pods. EDX analysis was performed to confirm the formation of silver nanoparticles with the elemental mapping. Observation of the characteristic peaks of silver, carbon, oxygen, and chlorine is made. The latter peaks, such as silica, aluminum, carbon, and oxygen, come from the phytochemicals present at the surface of the nanosilver, while chlorine is contained in AgCl nanoparticles. Table 2 summarizes all the chemical elements found in AgNPs as well as their mass and atomic concentration. A mixture of silver and silver chloride has been obtained using *Selaginela myosorus* plant extract. [29]. Two peaks located at the binding energy of 1.5 KeV belonging to aluminum were observed as well as that of Silicon at 1.7 KeV. Furthermore, the sample contained a high concentration of silver nanoparticles and a high atomic percentage.

3.2.6. X-Ray Diffraction of Nanoparticles from Aqueous Extract of Fresh Cocoa Pods and Silver Nanoparticle-Mediated Fresh Cocoa Pods. Figure 9 shows the diffractogram obtained from the fresh cocoa pods (a) and silver nanoparticles (b). The diffractogram of fresh raw cocoa pods shows wide diffraction lines of an amorphous structure. The PXRD pattern of the synthesized silver nanoparticles presents a crystalline peak at a 2θ value of 37.8° that can be indexed to the plane (111) of the face-centred cubic structure (JCPDS file: 65–2871). The PXRD pattern also showed the presence of the cubic phase of silver chloride at 2θ values of 27.8°, 32.3°, 46.2°, 54.8°, 57.4°, and 76.7° corresponding to the (111, 200, 220, 311, 222) and (420) planes, respectively (JCPDS file: 31–1238) (Table 3). The calculated average crystalline particle size was found to be 17.60 and 30.40 nm for silver and silver chloride, respectively, using the Debye–Scherrer equation (1) [16] (equation (1)):

$$\mathrm{Dv} = \left(\frac{K\lambda}{\beta\cos\theta}\right), \tag{1}$$

where Dv is the average crystalline size; K is a dimensionless shape factor, with a value close to unity (0.99); λ is the wavelength of CuKα; β is the full width at half-maximum of the diffraction peaks; and θ is Bragg's angle.

The average crystallinity size is 30.40 nm for AgCl and 17.60 nm for Ag. The diffraction pattern also shows unidentified crystalline phases of silver at 23.10, 34.50, and 42.80 positions of 2θ.

3.3. Electrochemical Characterization of Silver Nanoparticles

3.3.1. Cyclic Voltammetry. The permeability and surface charge of the material were evaluated by cyclic voltammetry (CV) at pH 2, 7, and 9 using [Fe $(CN)_6]^{3-}$, [Ru $(NH_3)_6]^{3+}$, and [Fe $(MeOH)_2$] as redox probes. Results for [Fe $(CN)_6]^{3-}$ shown in Figures 10(a) and 10(b) prove the efficiency of the nanoparticles synthesized in this work, which are performant in acid, neutral, and base media when drop-coated on GCE in comparison to the peak current obtained with the bare GCE. The system is fast and enhanced in neutral medium compared to the acidic or basic medium. Moreover, the silver nanoparticle film deposited on the surface of the GCE presents a parasitic oxidation signal, which appears around 0.03 V. The presence of this parasitic signal is due to the oxidation of silver metal present in the nanoparticles.

Analysis of the [Ru $(NH_3)_6]^{3+}$ ion has also been achieved, and the results are shown in Figures 10(c) and 10(d). As in the case of ferricyanide, the system for ruthenium hexamine is also reversible with bare GCE, and when modified with AgNPs, the background currents for oxidation and reduction are similar to those of GCE, even if the peaks are not well defined.

When using a neutral redox probe ([Fe $(MeOH)_2$]), the modified GCE remained higher in intensity and faster than bare GCE at different pH, as shown in the Figures 10(e) and 10(f). The results obtained from this characterization confirm that silver nanoparticles based on fresh cocoa pods are very porous conductor and can fix mostly negative and

TABLE 2: Elemental analysis of silver nanoparticles based on *Theobroma cacao*.

Element number	Element symbol	Element name	Atomic conc.	Weight conc.
47	Ag	Silver	10.14	45.91
8	O	Oxygen	38.91	26.13
6	C	Carbon	47.92	24.16
14	Si	Silicon	1.24	1.46
17	Cl	Chlorine	0.85	1.27
13	Al	Aluminum	0.94	1.07

TABLE 3: Main characteristics of the diffractogram of the nanoparticles obtained with the aqueous extract of *Theobroma cacao*.

No.	Pos. (°2Th.)	d-spacing (Å)	Height (cts)	FWHM left (°2Th.)	Plane	Size (nm)
1	27.896	3.196	38.010	0.312	111	27.410
2	32.303	2.769	100.240	0.281	200	30.780
3	37.896	2.372	29.620	0.499	111	17.580
4	46.282	1.960	100.970	0.250	220	36.170
5	54.860	1.672	28.360	0.374	311	24.980
6	57.510	1.601	37.230	0.250	222	34.940
7	76.784	1.240	29.430	0.374	420	28.290
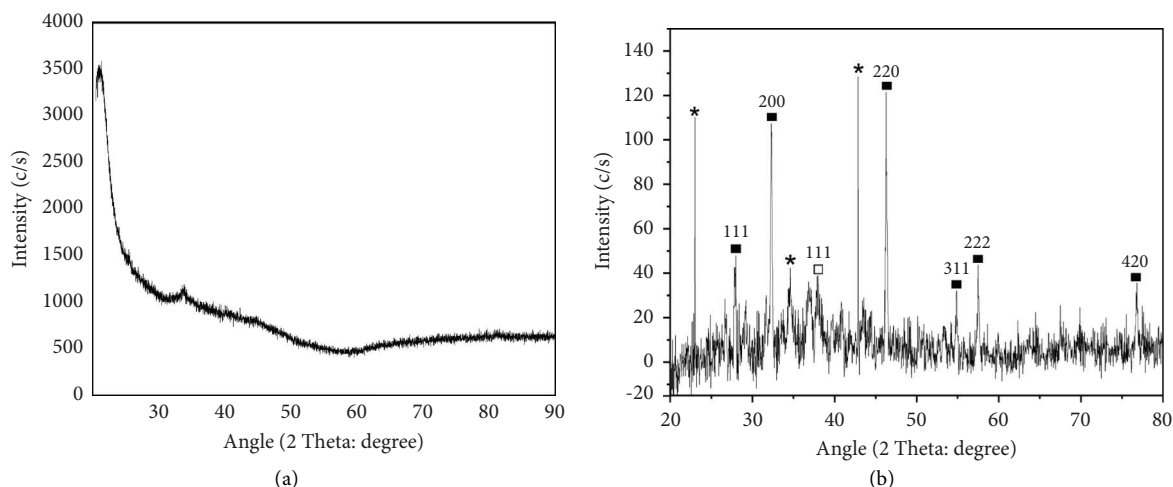
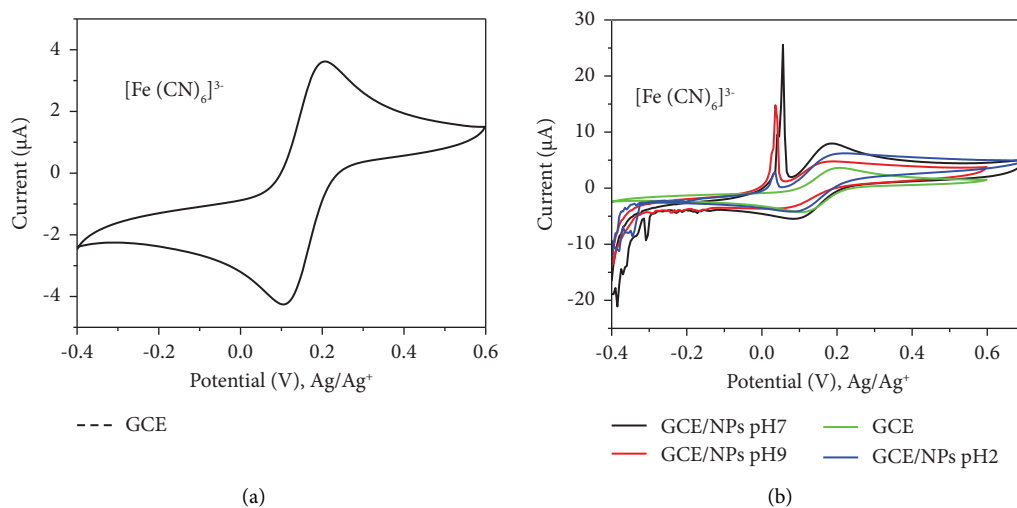FIGURE 9: X-ray diffractogram of fresh cocoa pods (a) and nanoparticles (b).
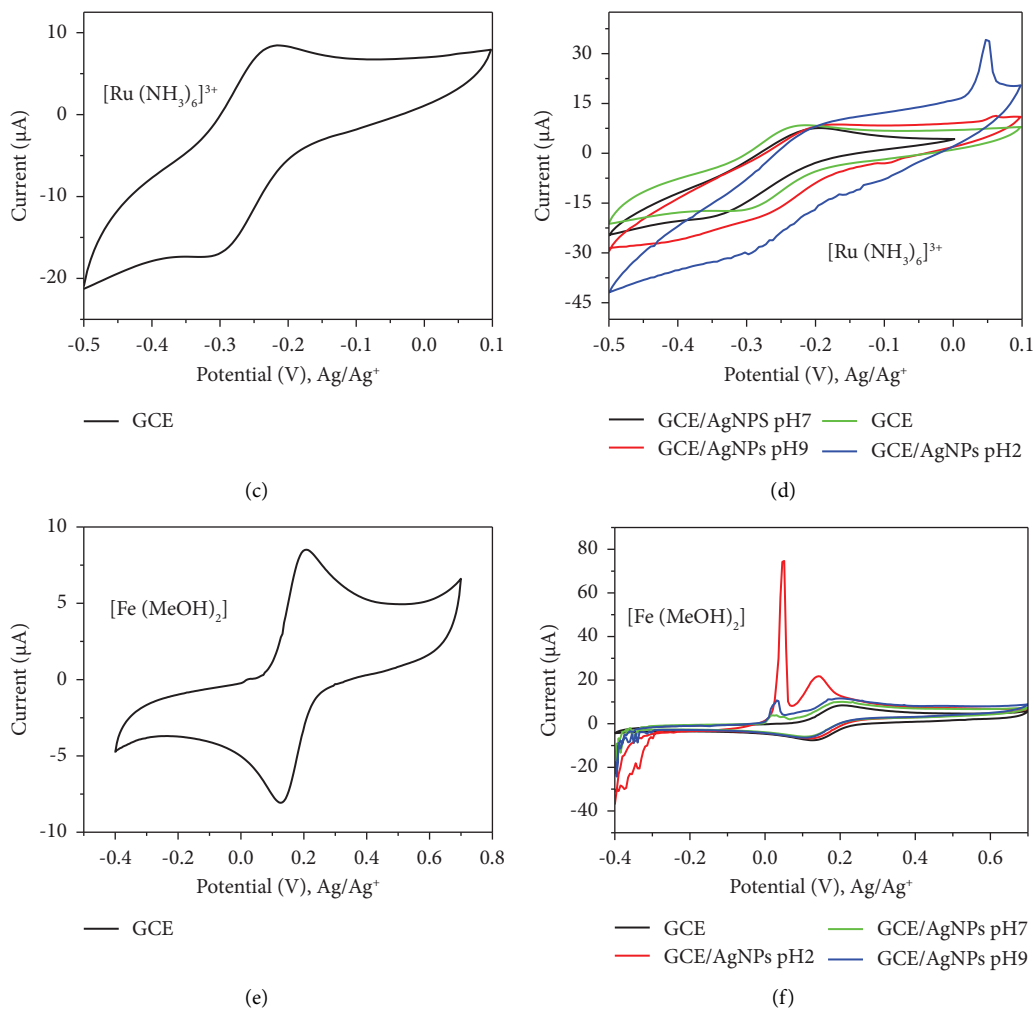

FIGURE 10: Continued.

(c)

GCE/AgNPS pH7 — GCE
GCE/AgNPs pH9 — GCE/AgNPs pH2

(d)

GCE

(e)

GCE   GCE/AgNPs pH7
GCE/AgNPs pH2   GCE/AgNPs pH9

(f)

FIGURE 10: Cyclic voltammograms obtained in a solution of 0.1 M KCl (pH 2, 7, and 9) and 5×10^{-3} M [Fe (CN)$_6$]$^{3-}$ (a, b), [Ru (NH$_3$)$_6$]$^{3+}$ (c, d), [Fe (MeOH)$_2$] (e, f) on different electrodes; scan rate: 50 mV/s.

neutral analytes in solution by electrostatic attraction and affinity phenomena, while repelling positive analytes. Thus, this result promotes the use of GCE/AgNPs as an electrochemical sensor for negative analytes in solution.

3.3.2. Electrochemical Impedance Spectroscopy. The results obtained from the Nyquist graph for GCE and GCE/AgNPs are presented in Figure 11. The electrolysis (Re) and charge transfer (Rt) resistance for bare GCE and GCE/AgNPs were Re = 0 kΩ, R_{ct} = 972.22 Ω, Re = 0 kΩ, and R_{ct} = 333.33 Ω, respectively. The low value of the R_{ct} obtained with GCE/AgNPs reflects a rapid electron transfer on GCE-AgNPs compared to GCE, which can be explained by the shielding of AgNPs by negatively charged [Fe (CN)$_6$]$^{3-/4-}$ in solution as previously demonstrated in CV.

3.3.3. Application of GCE/AgNPs to the Simultaneous Detection of Ascorbic Acid and Uric Acid. GCE/AgNPs have been applied for the simultaneous detection of ascorbic acid (AA) and uric acid (UA). Figure 12 shows the electrochemical behavior of ascorbic acid towards uric acid in the buffer solution of Briton Robinson at pH 7 using unmodified GCE in the absence of ascorbic and uric acid (green). Analysis of this figure reveals the presence of an oxidation peak centred at 0.30 V with GCE reflecting the oxidation of ascorbic acid or uric acid or both. On the other hand, for GCE/AgNPs, two peaks of oxidation potential are observed around 0.37 V and 1.13 V corresponding, respectively, to ascorbic acid and uric acid [30]. This result confirms the effectiveness of AgNPs against negatively charged analytes in solution, and the good electrocatalytic behavior of the fabricated electrode, as shown in Table 4 where the comparison in terms of the potential difference between ascorbic acid and uric acid is given with the different sensors. The mechanism of their oxidation is given by Scheme 1.
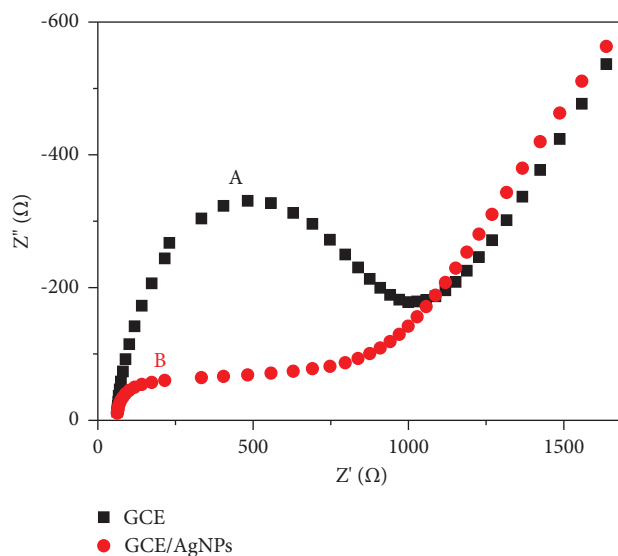
FIGURE 11: Nyquist diagram recorded by the electrochemical impedance spectroscopy in medium 10^{-3} M [Fe (CN)$_6$]$^{3-/4-}$ and 0.1 M KCl (pH 7) on two electrodes: GCE-naked (A), GCE-AgNPs (B).
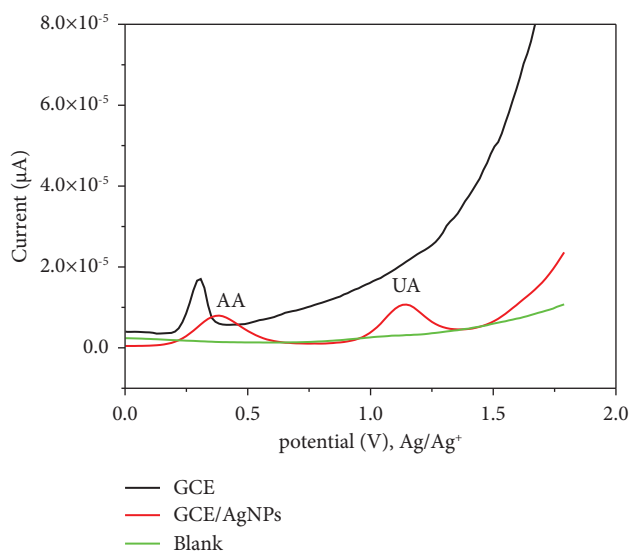

FIGURE 12: Differential pulse voltammograms of 10^{-4} M ascorbic acid (AA) and uric acid (UA) in a Briton Robinson buffer solution at pH 7 recorded on GCE and GCE/AgNPs electrodes.

TABLE 4: Comparison of the potential difference of AA-UA using different electrodes.

Methods	Electrodes	Potential difference (V)	References
DPV	CPC/GCE	0.40	[31]
DPV	PAN-ABSA/GCE	0.30	[32]
DPV	PAN-OAP/GCE	0.35	[33]
CV	MCNTPE/CMF	0.40	[33]
DPV	GCE/AgNPs	0.75	This work

CPC, cetylpyridinium chloride; MCNTPE, multiwall carbon nanotube-paste electrode; CMF, chloromercuriferrocene; PAN, polyaniline; ABSA amino-benzene sulfonic acid (ABSA); OAP, o-aminophenol.
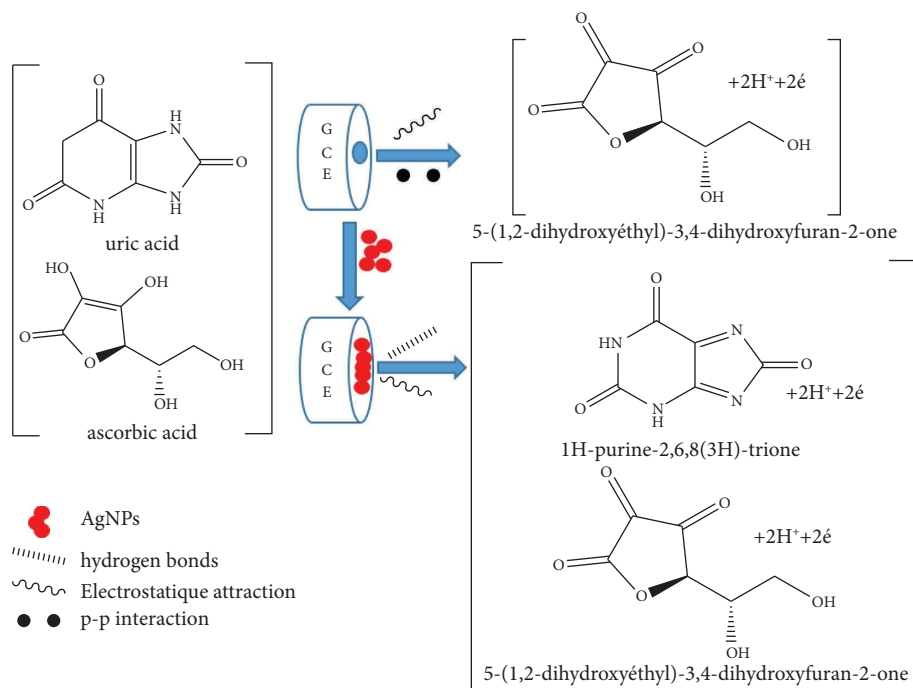
Scheme 1: Proposed mechanism of the interaction between GCE/AgNPs and the two analytes.

4. Conclusion

The synthesis and characterization of silver nanoparticles based on extracts of fresh cocoa pods have been reported. The pH, incubation time, and concentration of silver nitrate greatly influence the formation of nanoparticles. Characterization methods such as UV-vis, FT-IR spectroscopy including structural (XRD) and morphological (SEM) studies suggest that fresh cocoa pod extract plays an essential role during the bioreduction of silver ions and in the stabilization of silver nanoparticles. Electrochemical characterizations have shown that silver nanoparticles based on extracts of *Theobroma cacao* can be used as an electrode material for the electroanalysis of negatively or neutrally charged analytes in solution, since the electrostatic interaction will be favorable between the ion metallic Ag$^+$ and the negatively charged analyte. Electrochemical impedance spectroscopy showed a low charge-transfer resistance to GCE/AgNPs, which involves a rapid electron transfer. The fabricated electrode shows a good electrocatalytic behavior for the separation of ascorbic acid and uric acid (around 0.60 V). This work allows us to propose a new axis of synthesis of electrode materials for various applications, in particular the simultaneous detection of certain organic compounds in drugs, which is currently being studied by our research team. [34].

Data Availability

Data are made available upon request to the corresponding author.

Conflicts of Interest

The authors declare that they have no conflicts of interest.

Authors' Contributions

Alex Vincent Somba performed formal analysis, proposed a methodology, performed an investigation, and wrote the original draft. Evangéline Njanja conceptualized the study, proposed a methodology, and wrote, validated, and supervised the study. Gullit Deffo performed formal analysis, proposed a methodology, performed an investigation, and wrote and edited the study. Cyrille Ghislain Fotsop proposed a methodology, performed characterization, and edited the study. Kevin Tajeu reviewed and edited the study. Armel Florian Tchangou Njiemou proposed a methodology and edited the study. François Eya'ane Meva conceptualised the study, reviewed, validated, and supervised the study, and administered the project. Théophile Kamgaing conceptualized the study, edited, validated, and supervised the study, and performed project administration.

References

[1] S. S. Suri, H. Fenniri, and B. Singh, "Nanotechnology-based drug delivery systems," *Journal of Occupational Medicine and Toxicology*, vol. 2, no. 1, p. 16, 2007.

[2] J. Huang, Q. Li, D. Sun, Y. Lu, Y. Su, and X. Yang, "Biosynthesis of silver and gold nanoparticles using a novel

sundried Cinnamomum camphora leaf," *Nanotechnology*, vol. 18, pp. 1–11, 2007.

[3] W. Al Zoubi, R. A. K. Putri, M. R. Abukhadra, and Y. G. Ko, "Recent experimental and theoretical advances in the design and science of high-entropy alloy nanoparticles," *Nano Energy*, vol. 110, Article ID 108362, 2023.

[4] M. M. Alam, A. M. Asiri, M. T. Uddin, M. A. Islam, M. R. Awual, and M. M. Rahman, "Detection of uric acid based on doped $ZnO/Ag_2O/Co_3O_4$ nanoparticle loaded glassy carbon electrode," *New Journal of Chemistry*, vol. 43, no. 22, pp. 8651–8659, 2019.

[5] S. D. Bansod, M. S. Bawaskar, A. K. Gade, and M. K. Rai, "Development of shampoo, soap and ointment formulated by green synthesised silver nanoparticles functionalised with antimicrobial plants oils in veterinary dermatology: treatment and prevention strategies," *Institution of Engineering and Technology Nanobiotechnology*, vol. 9, no. 4, pp. 165–171, 2015.

[6] T. Benn, B. Cavanagh, K. Hristovski, J. D. Posner, and P. Westerhoff, "The release of nanosilver from consumer products used in the home," *Journal of Environmental Quality*, vol. 39, no. 6, pp. 1875–1882, 2010.

[7] M. Rai, A. Yadav, and A. Gade, "Silver nanoparticles as a new generation of antimicrobials," *Biotechnology Advances*, vol. 27, no. 1, pp. 76–83, 2009.

[8] Y. Park, "A new paradigm shift for the green synthesis of antibacterial silver nanoparticles utilizing plant extracts," *Toxicological Research*, vol. 30, no. 3, pp. 169–178, 2014.

[9] K. N. Thakkar, S. S. Mhatre, and R. Y. Parikh, "Biological synthesis of metallic nanoparticles," *Nanomedicine: Nanotechnology, Biology and Medicine*, vol. 6, no. 2, pp. 257–262, 2010.

[10] P. C. Ray, H. Yu, and P. P. Fu, "Toxicity and environmental risks of nanomaterials: challenges and future needs," *Journal of Environmental Science and Health, part C.*, vol. 27, pp. 1–35, 2009.

[11] E. R. A. M. Fran ccedil ois, L. S. Marcelle, O. E. Cecile et al., "Unexplored vegetal green synthesis of silver nanoparticles: a preliminary study with Corchorus olitorus Linn and Ipomea batatas (L.) Lam," *African Journal of Biotechnology*, vol. 15, no. 10, pp. 341–349, 2016.

[12] M. Dubey, S. Bhadauria, and B. S. Kushwah, "Green synthesis of nanosilver particles from extract of Eucalyptus hybrid (Safeda) leaf. Digest," *Journal. Nanomaterials and Biostructures*, vol. 4, pp. 537–543, 2009.

[13] H. Gebru, A. Taddesse, J. Kaushal, and O. P. Yadav, "Green synthesis of silver nanoparticles and their antibacterial activity," *Journal of Surface Science and Technology*, vol. 29, pp. 47–66, 2013.

[14] A. Leela and M. Vivekanandan, "Tapping the unexploited plant resources for the synthesis of silver nanoparticles," *African Journal of Biotechnology*, vol. 7, pp. 3162–3165, 2008.

[15] D. MubarakAli, N. Thajuddin, K. Jeganathan, and M. Gunasekaran, "Plant extract mediated synthesis of silver and gold nanoparticles and its antibacterial activity against clinically isolated pathogens," *Colloids and Surfaces B: Biointerfaces*, vol. 85, no. 2, pp. 360–365, 2011.

[16] G. Deffo, M. Basumatary, N. Hussain et al., "Eggshell nano-$CaCO_3$ decorated PANi/rGO composite for sensitive determination of ascorbic acid, dopamine, and uric acid in human blood serum and urine," *Materials Today Communications*, vol. 33, Article ID 104357, 2022.

[17] G. Deffo, R. Hazarika, M. C. Deussi Ngaha et al., "An ultrasensitive uric acid second generation biosensor based on chemical immobilization of uricase on functionalized multiwall carbon nanotube grafted palm oil fiber in the presence of a ferrocene mediator," *Analytical Methods*, vol. 15, no. 20, pp. 2456–2466, 2023.

[18] M. M. Hussain, M. M. Rahman, A. M. Asiri, and M. R. Awual, "Non-enzymatic simultaneous detection of L-glutamic acid and uric acid using mesoporous Co_3O_4 nanosheets," *RSC Advances*, vol. 6, no. 84, pp. 80511–80521, 2016.

[19] M. M. Rahman, M. M. Hussain, and A. M. Asiri, "Enzyme-free detection of uric acid using hydrothermally prepared $CuO \cdot Fe_2O_3$ nanocrystals," *New Journal of Chemistry*, vol. 44, no. 45, pp. 19581–19590, 2020.

[20] Y. Xue, Y. Zheng, E. Wang, T. Yang, H. Wang, and X. Hou, "$Ti_3C_2T_x$ (MXene)/Pt nanoparticle electrode for the accurate detection of DA coexisting with AA and UA," *Dalton Transactions*, vol. 51, no. 11, pp. 4549–4559, 2022.

[21] F. Eya'ane Meva, M. L. Segnou, C. Okalla Ebongue et al., "Spectroscopic synthetic optimizations monitoring of silver nanoparticles formation from Megaphrynium macrostachyum leaf extract," *Revista Brasileira de Farmacognosia*, vol. 26, no. 5, pp. 640–646, 2016.

[22] Z. Baharum, A. Akim, Y. Taufiq-Yap, R. Hamid, and R. Kasran, "*In vitro* antioxidant and antiproliferative activities of Methanolic Plant Part Extracts of Theobroma cacao," *Molecules*, vol. 19, no. 11, pp. 18317–18331, 2014.

[23] F. Eya'ane Meva, M. L. Segnou, C. Okalla Ebongue, D. Vandi, N. Ngo, and E. A. Mpondo Mpondo, "Synthesis, optimization and effect of condition reactions studies of seed kernel aqueous extract mediated silver nanoparticles from Ricinodendron heudelotii (Baill) Pierre Pax," *International Journal of Biosciences*, vol. 7, pp. 45–56, 2015.

[24] M. M. H. Khalil, E. H. Ismail, K. Z. El-Baghdady, and D. Mohamed, "Green synthesis of silver nanoparticles using olive leaf extract and its antibacterial activity," *Arabian Journal of Chemistry*, vol. 7, no. 6, pp. 1131–1139, 2014.

[25] S. Chandran, M. Chaudhary, R. Pasricha, A. Ahmad, and M. Sastry, "Synthesis of gold nanotriangles and silver nanoparticles using Aloe vera plant extract," *Biotechnology Progress*, vol. 22, no. 2, pp. 577–583, 2006.

[26] G. Mie, "Beiträge zur optik trube Medien, speziell kolloidaler Metallösunger," *Annals of Physics*, vol. 330, pp. 345–377, 1908.

[27] J. Kasthuri, S. Veerapandian, and N. Rajendiran, "Biological synthesis of silver and gold nanoparticles using apiin as reducing agent," *Colloids and Surfaces B: Biointerfaces*, vol. 68, no. 1, pp. 55–60, 2009.

[28] G. Cruz, M. Pirila, M. Huuhtanen, L. Carri € on, and E. Alvarenga, "Production of activated carbon from cocoa (theobroma cacao) pod husk," *Journal of Civil and Environmental Engineering*, vol. 02, no. 02, p. 109, 2012.

[29] P. Belle Ebanda Kedi, F. Eya'ane Meva, L. Kotsedi et al., "Eco-friendly synthesis, characterization, in vitro and in vivo anti-inflammatory activity of silver nanoparticle-mediated *Selaginella myosurus* aqueous extract," *International Journal of Nanomedicine*, vol. 13, pp. 8537–8548, 2018.

[30] K. Barman and S. K Jasimuddin, "Simultaneous electrochemical detection of dopamine and epinephrine in presence of ascorbic acid and uric acid using AgNPs-penicillamine-Au electrode," *Royal Society of Chemistry Advances*, vol. 6, pp. 1–6, 2016.

[31] A. P. D. Reis, C. R. T. Tarley, and L. T. Kubota, "Micelle-mediated method for simultaneous determination of ascorbic acid and uric acid by differential pulse voltammetry," *Journal of the Brazilian Chemical Society*, vol. 19, no. 8, pp. 1567–1573, 2008.

[32] L. Zhang, C. Zhang, and J. Lian, "Electrochemical synthesis of polyaniline nano-networks on p-aminobenzene sulfonic acid functionalized glassy carbon electrode," *Biosensors and Bioelectronics*, vol. 24, no. 4, pp. 690–695, 2008.

[33] L. Zhang and L. L. Wang, "Electrochemical synthesis of a polyaniline Network on a poly(o-aminophenol) modified glassy carbon electrode and its use for the simultaneous determination of ascorbic acid and uric acid," *Analytical Sciences*, vol. 28, no. 10, pp. 1001–1007, 2012.

[34] R. akbari, M. noroozifar, M. khorasani-Motlagh, and A. Taheri, "Simultaneous determination of ascorbic acid and uric acid by a new modified carbon nanotube-paste electrode using chloromercuriferrocene," *Analytical Sciences*, vol. 26, no. 4, pp. 425–430, 2010.